Fabricating optical fibre-top cantilevers for temperature sensing

Fabricating optical fibre-top cantilevers for temperature sensing

2014 Meas. Sci. Technol. 25 035206

(http://iopscience.iop.org/0957-0233/25/3/035206)

OPEN ACCESS
IOP Publishing
Measurement Science and Technology
Meas. Sci. Technol. **25** (2014) 035206 (9pp)
doi:10.1088/0957-0233/25/3/035206

Fabricating optical fibre-top cantilevers for temperature sensing

J Li[1], F Albri[1], J N Sun[2], M M Miliar[2], R R J Maier[1], D P Hand[1] and W N MacPherson[1]

[1] Institute of Photonics and Quantum Sciences, SUPA, Heriot-Watt University, Edinburgh, EH14 4AS, UK
[2] Institute of Mechanical, Process and Energy Engineering, Heriot-Watt University, Edinburgh, EH14 4AS, UK

E-mail: jl294@hw.ac.uk

Received 2 September 2013, revised 25 December 2013
Accepted for publication 8 January 2014
Published 17 February 2014

Abstract

In this paper, we propose techniques to fabricate micro-cantilevers onto the end of standard single mode optical fibres using a combination of picosecond laser machining and focused ion beam milling techniques and demonstrate their use as temperature sensors. Using this approach the cantilever can be pre-aligned with the core of the fibre during fabrication, therefore offering a stable and straightforward means of optically addressing the cantilever. The cantilever is designed to measure deflection over a range of 10 μm using a simple readout technique. A phase recovery algorithm is employed to reduce the interrogation error to around 2–3 nm. Finally, a temperature cycling experiment demonstrates that the cantilever could be used as a temperature sensor from room temperature to 500 °C with an average rms temperature error from 20 °C to 500 °C of $\sim \pm 1.4$ °C.

Keywords: micro-machining, optical fibre cantilever, temperature sensing, focused ion beam

(Some figures may appear in colour only in the online journal)

1. Introduction

Temperature measurement is a well-established field of research with interest in temperature sensing ranges from tens of degrees to over a thousand degrees Celsius [1–3]. Currently, high temperatures (>500 °C) can be measured using thermocouples and these are widely available. However, for temperature sensing within a constrained space, or in the presence of electrical noise, these sensors have some limitations. Therefore, there has also been significant effort in developing optical fibre sensors for space constrained and harsh environment temperature sensing applications. Typically, they use micro-machining techniques or material deposition techniques to fabricate a Fabry–Perot (FP) cavity into an optical fibre. Temperature measurement is achieved by monitoring the changing of refractive index and/or physical length of the cavity as the environment temperature varies [4]. Similar approaches have been demonstrated using a sapphire fibre with a reported maximum temperature measured up to 1600 °C [5]. Another approach to high temperature sensing uses fibre Bragg gratings (FBG), but special effort is needed to make these stable at elevated temperatures [6] by careful selection of thermal and grating writing recipes. More recently re-generated FBGs have shown to be able to operate up to near the glass softening temperature [7]; however, the re-generation process often results in mechanically weak fibres.

Micro-cantilever sensors have recently attracted attention as promising and highly sensitive devices for micron scale mechanical transducers. Pioneering work by Ianuzzi *et al* used focused ion beam (FIB) machining to fabricate fibre-top cantilever structures onto the end of an optical fibre [8]. This demonstrates a 'plug-and-play' device that combines the sensing element (cantilever) and interrogation optics (via the fibre core) as a single element probe which can be used in a wide range of applications. Such structures are capable of detecting any small deflection induced by a mechanical force applied to a cantilever beam, thus making it useful for

industrial, biological, chemical and other sensing applications [9–13]. There is also a possibility of using micro-cantilevers to measure temperature change based on differential thermal expansion, similar to the 'bimetallic effect' [14]. In this case, the cantilever converts the thermally induced deflection of a multi-material cantilever beam of submillimetre size into a measurable signal, for example an electrical signal through tunnelling current modulation [15] or the piezoelectric effect [16]. These devices are generally small and offer potential advantages for space constrained applications.

Cantilever-based temperature sensing has been reported. For example, Spietz *et al* [17] used such an approach to exploit the shot noise in a tunnel junction to measure very low temperature. The approach is highly sensitive, however, electronic-based devices are affected by electrical noise interference and the operating temperature range may be limited by the materials used. Optical readout methods have also been reported. Wu *et al* [18] presented an optical beam deflection method to measure temperature based on the bimetallic cantilever beam structure and demonstrate a temperature sensitivity of 0.02 K, however, in this case, the readout system is bulky and the alignment of laser beam to the cantilever is not straightforward. In addition, the dimension of the sensing probe of around 1 mm limits the use in some micro-scale applications.

In this paper, we propose an optical fibre-based cantilever to address the issues identified above. A range of approaches to fabricate such sensors have been reported in the open literature. FIB techniques used to fabricate early devices [8] offer great control of feature dimensions down to the nm level, with excellent surface finish, but are slow. Alternative techniques using femtosecond (fs)-laser exposure and subsequent etching [12] or using photolithography techniques [13] hold great promise for producing the required features using processes that are faster, and have potential for mass fabrication. Direct laser machining of ferrule-top cantilevers has also been demonstrated [19]. In our work, we wish to exploit the benefits of direct laser machining to produce a single material cantilever. The cantilever structure is machined directly onto the end of a standard single mode fibre by using a picosecond (ps)-laser and further processed using FIB machining techniques. Using fused silica fibres allows sensor operation in harsh environments and at elevated temperatures compared to many electrical-based sensors. Compared with other all-silica fabrication techniques such as fs laser machining combined with HF etching or FIB only machining, the total machining time is reduced and this makes it potentially suitable for industrial production.

In our experiments, an algorithm based upon the fast Fourier transform (FFT) is used to determine an approximate cavity length and then a least mean square phase recover algorithm is employed to refine the measurement of cantilever deflection. A cavity length measurement with a resolution around 2–3 nm has been achieved for a stabilized cantilever. Finally, temperature sensing is demonstrated with a sensing range up to 500 °C and responsivity of 40.2 nm $^{\circ}C^{-1}$ and demonstrated rms temperature error of $\sim \pm 1.4$ °C.

2. Fabrication of fibre-top micro-cantilevers

2.1. ps-laser machining

A commercial ps-laser system (Trumpf TruMicro 5 × 50) with a wavelength of 343 nm is used during the first stage of fabricating cantilevers onto the end of single mode optical fibres. Our approach allows up to ten fibres to be machined in close succession, but demonstrates the potential for large scale manufacture. The laser processing is performed using 6 ps pulses with energy of 10 μJ per pulse and a focused spot of 6 μm diameter. The beam is focused on the work piece via a galvanometer (galvo) scan head to quickly and accurately move the focused spot across the fibre. In our experiments, the laser beam is translated at up to 100 mm s^{-1} with a pulse repetition rate of 40 kHz. An *in-situ* microscope is used for detailed process monitoring.

The machining process is illustrated in figure 1. First, the fibres are cleaved, cleaned and then mounted in a V-groove holder. Then the laser beam ablates the top cleaved surface of the fibre and removes material from the side of fibre. The fibre is then rotated to allow the cantilever to be fabricated from this ridge by removing a section beneath it, as shown in figure 1(*b*). It should be noted in this stage it is important to control the alignment of the machined surface, which will form the reflective surface of the cavity. During this laser cutting process, a rotation mount allows the fibre to be aligned appropriately to compensate for the tapering angle caused by the laser beam profile. The resulting cantilever is shown in figure 1(*d*), which is 110 μm long, 18 μm wide and 8 μm thick. These dimensions are approaching the limitation of our fabrication process primarily due to error of mechanical alignment and laser positioning error. The detailed machining process is discussed in earlier work [20, 21].

2.2. Focused ion beam polishing

FIB milling [22] is used to reduce the cantilever thickness in order to improve the mechanical sensitivity. After the laser machining process, the machined cantilever was coated with a 20 nm gold layer in order to reduce electrostatic charge accumulation during the FIB process. The FIB machining was carried out on a dual-beam FIB system (FEI Quanta 3D FEG). A liquid gallium ion source and a field emission scanning electron microscope (SEM) were available in the system. The cantilever fibres remained on the same mounting block used in the laser processing to avoid any misalignment during transit between machining stations. The FIB stage supporting the mounting block can tilt in the electron–ion beam plane from −15° to +75° with a minimum of 0.1° increments with the prepared cantilevers aligned horizontally on the stage. The stage was tilted to 52.0° at the eccentric height to ensure correct alignment relative to the ion beam axis. The SEM was placed to the fibre side for real-time monitoring of the fabrication process.

The milling process starts with a beam acceleration voltage of 30 keV and a current of 15 nA. A narrow rectangular pattern of 110 μm long and 2 μm wide is used to thin the cantilever as shown in figure 2(*a*). The pattern is aligned

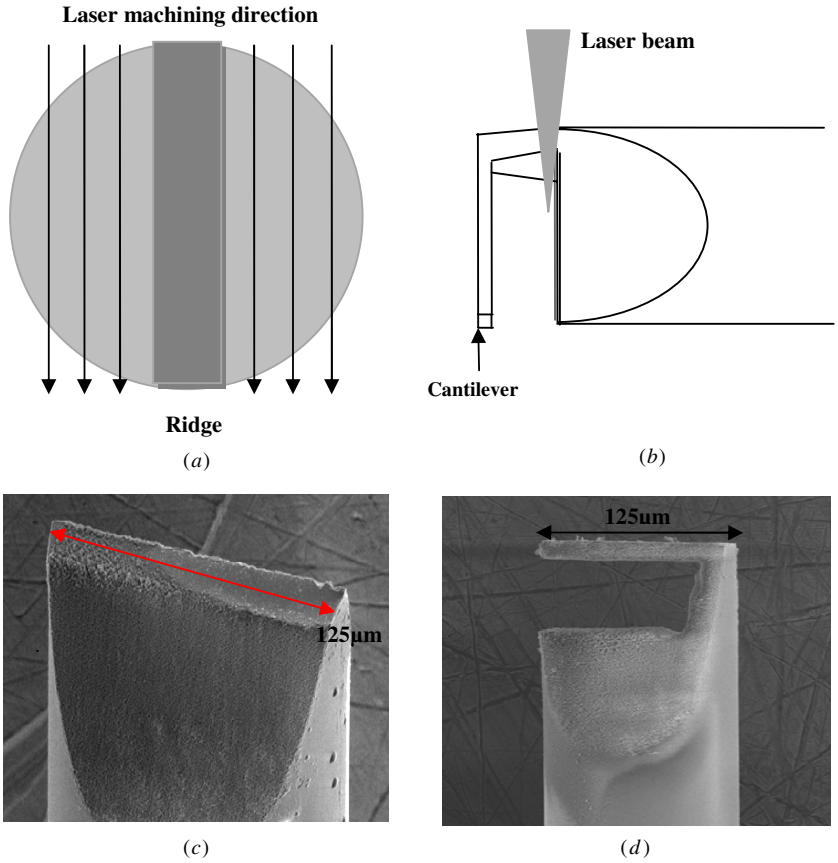

Figure 1. Outline laser machining process to form fibre-top cantilever, (*a*) ps-laser machine a ridge onto cleaved fibre (top view), (*b*) ps-laser under-cut to form free standing cantilever (side view), (*c*) SEM view of machined ridge and (*d*) SEM view of ps-laser machined cantilever.

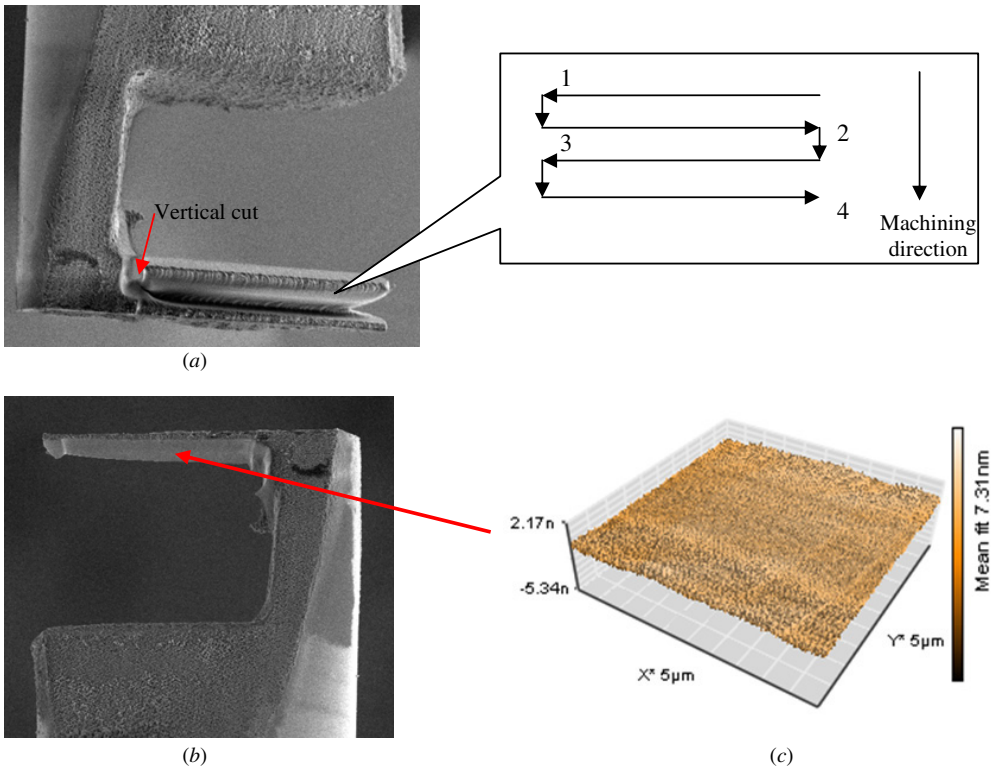

Figure 2. (*a*) FIB polishing process. (*b*) Final optical fibre cantilever after FIB processing. (*c*) Surface roughness of bottom cantilever surface under AFM.

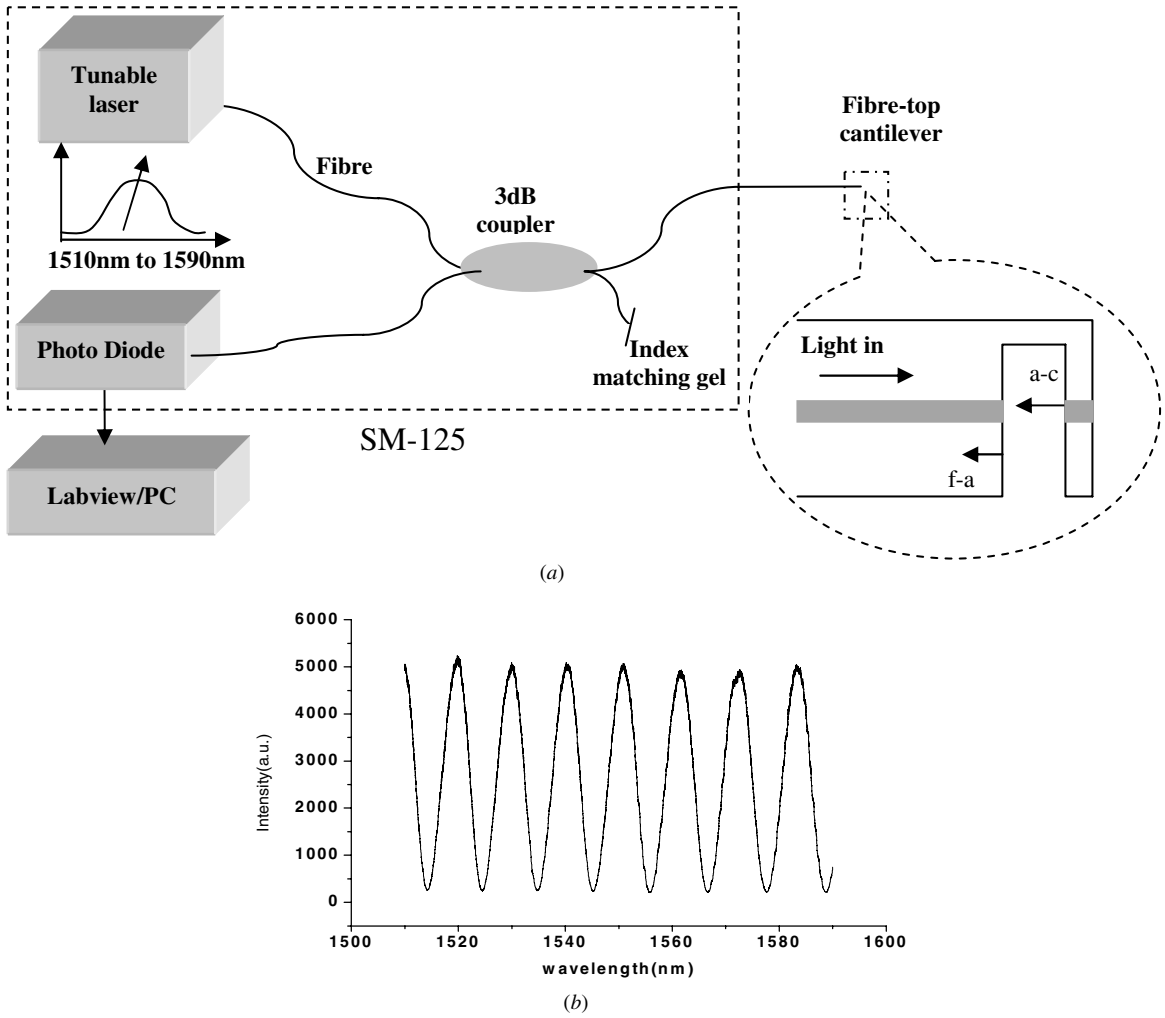

Figure 3. (*a*) Experimental set-up of interrogation system. (*b*) Normalized interference fringes.

such that the ion beam first machines a parallel cut with respect to the cantilever. The cut is not complete all the way around the section to be removed; instead we leave a small connection with the main part. This approach forms a temporary 'shield' between the cantilever and the fibre core and is used to mitigate against material re-deposition onto the cantilever bottom surface during an FIB polishing of the core surface. Then a second cut around the hinge perpendicular to the cantilever is used to release the 'shield', thus forming the final cantilever.

This laser/FIB dual process reduces the polishing time down to less than 20 min for cantilevers of these dimensions after ps-laser machining, a significant reduction in FIB machining compared with forming the complete structure using FIB. The resulting cantilever is shown in figure 2(*b*). In order to verify the surface finish of the final polished cantilever, an AFM is used to investigate the surface quality. Figure 2(*c*) shows the topography of the inner cantilever surface. The surface roughness (R_a) of FIB machined surface is measured to be in the nm range. This step provides the high quality reflective surfaces that offer an improved FP interferogram for measuring cantilever deflection.

3. Optical fibre interrogation

3.1. Interrogation system

The experimental set-up of the optical fibre cantilever interrogation system is shown in figure 3(*a*), where we use SM-125 interrogator from MicroOptics to measure the cavity reflection spectrum. The incident light from the SM-125 tunable laser is partially reflected at the fibre-to-air (f-a) and air-to-cantilever (a-c) surface. The reflected signal is recovered by a splitter internal to the SM-125. We use proprietary LabView routines to process the interferogram to yield the final gap length between the (a-c) and (f-a) surfaces.

A typical interferogram is shown in figure 3(*b*). The measured intensity I_R can be approximated by the approach described in [23]:

$$I_R = I_0\left[R_1 + \eta^2 R_2(1-R_1)^2 + 2\eta\sqrt{R_1R_2(1-R_1)}\cos\left(\frac{4\pi nL}{\lambda}\right)\right], \quad (1)$$

where I_0 is the input light intensity, R_1, R_2 are reflection of the two surfaces, and η takes into account the effect of beam divergence in the free space cavity [25]. Assuming low

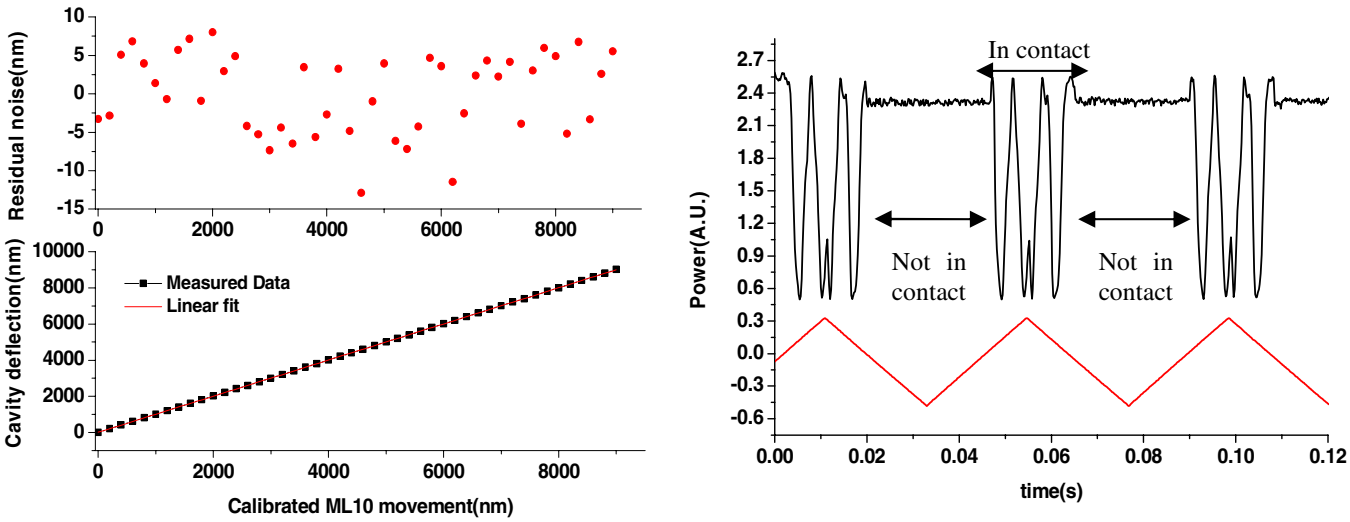

Figure 4. (*a*) Measured cavity length versus movement of ML10. (*b*) Dynamic response of micro-machined cantilever: top trace shows return from the cavity monitored at a single wavelength, bottom trace shows the piezo driving voltage which will approximate the piezo stage displacement.

reflectivity, then equation (1) can be simplified to the following equation:

$$I_R = I_0\left[1 + V\cos\left(\frac{4\pi nL}{\lambda}\right)\right]. \quad (2)$$

In equation (2), V is the cavity visibility which can be related to R_1, R_2 and η. In our experiment, wavelength information is converted to the frequency domain and an FFT is used to find the frequency peak which is directly related to the free spectral range and hence the cavity length.

3.2. Cantilever calibration

To test the behaviour of the cantilever as a micro-displacement sensor, the cantilever is mounted onto a translation stage. A second fibre is used as an actuator approaching the cantilever tip to apply a small known displacement. The movement of the actuator is controlled using a piezoelectric driven translation stage. For calibration purpose, a Renishaw ML10 position sensor with a resolution of 1 nm is used to monitor the position of piezoelectric translation stage. By using the similar interrogation technique discussed in 3.1, experimental data is acquired and processed. Figure 4(*a*) shows the measured cantilever deflection up to 9000 nm with a near linear response. The maximum residual error of the cavity length (compared with the ML10) is around 10 nm and a calculated rms error is ± 8.9 nm, which means our interrogation system is capable of detection cantilever deflection change of a few nanometres. A different single wavelength laser-based interrogation system [23] is used to acquire time resolved optical signals when we apply a triangular voltage ramp to the piezo-electric stage. As shown in figure 4(*b*), the response signals from a single wavelength interrogation of a FP cavity is cosinusoidal while the actuating fibre is in contact with the cantilever and displacing it over several fringes, as we would expect.

3.3. Phase recovery algorithm to improve resolution

The spectral domain technique [24, 25] used here is a common way for determining the cavity length from an interferogram. For precise measurement, the accuracy and sensitivity usually depend on the parameters of sensor itself and spectral signal processing. Here, we propose an additional phase recovery method to improve the accuracy of cavity length and minimize the noise that will ultimately degrade the sensor performance.

We know that when transferring the interferogram to optical frequency domain by FFT, the real part allows us to determine free spectral range. Therefore, we should be able to further enhance our measurement by considering the phase of the interferogram in addition to the free spectral range.

In our system, using the FFT approach, we are able to determine the cavity length to better than one fringe; however, we are unable to resolve very small changes in cavity length. For high sensitivity measurement, missing this small change may lead to significant error. We aim to recover this phase information by finding the best fit between the real interferogram and a modelled interferogram generated using the FFT cavity length as a starting point. First, we use cavity length L, determined from the FFT algorithm applied to the experimental data to produce model FP interference fringes based on equation (2). A small wavelength shift is evident between the measured and modelled spectrum, which is shown in figure 5(*a*). A least mean squares algorithm is used to find the minimum error position between the modelled and experimental cavity for small variations in the cavity length. Figure 5(*b*) shows the least square mean error between the model and experimental spectrum as a function of varying the modelled cavity length. The minimum indicates the required correction to be applied to the original FFT determined cavity length. Figure 5(*c*) shows the improvement between the modelled spectrum based on this revised cavity length after using phase recovery algorithm and the experimental spectrum. Figure 5(*d*) shows the effect of the improvement by comparing the noise before and after applying this phase

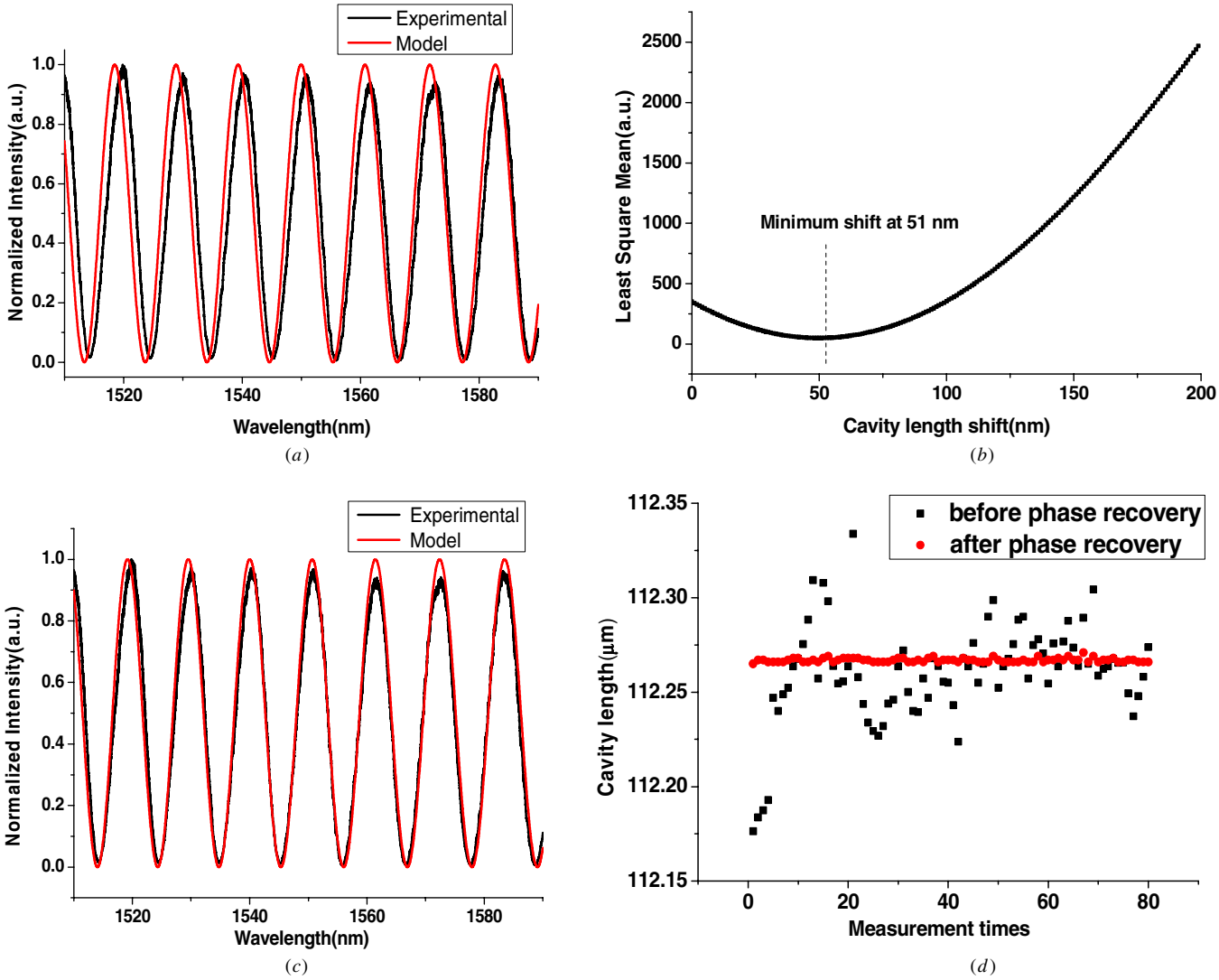

Figure 5. (*a*) Experimental spectrum and model based on starting cavity length recovered from FFT algorithm. (*b*) Plot of least mean squares fit between experimental and modelled data versus a small shift in cavity length around the FFT value. (*c*) Comparison between model and experimental after phase recover process applied. (*d*) Noise measurement over 80 scans for a stabilized cavity length before and after phase recovery algorithm.

recovery algorithm when testing a static cantilever; here, the absolute cavity length fluctuation is reduced by nearly ten times. The maximum cavity length deviation after applying the phase recovery algorithm is within 2–3 nm, with an rms error of 0.87 nm, based on data in figure 5(*d*). This means the cavity length error produced by the initial FFT algorithm can be reduced to nanometre scale by using phase information contained in the interferogram.

4. Temperature sensing experiment

To make the cantilever temperature sensitive, we apply a thin metallic layer to the top surface of a fibre-top cantilever. The different thermal expansion between the fused silica cantilever and the coating material results in a deflection that is related to the temperature. The sensor configuration is shown in figure 6(*a*).

4.1. Model analysis of bimetallic effect

Similar to the bimetallic effect [26], the thermal coefficient of expansion mismatch between the two components of a sandwiched layer can be used to provide displacement as a function of temperature. A fused silica cantilever with a metal layer coated on one surface will generate a tip deflection due to the temperature change. The deflection of the cantilever beam could be written by the following equation presented in [26]:

$$k = \frac{1}{r} = \frac{6b_1b_2E_1E_2t_1t_2(t_1+t_2)(a_2-a_1)\Delta T}{\left(b_1t_1^2E_1\right)^2+\left(b_2t_2^2E_2\right)^2+2b_1t_1E_1b_2t_2E_2\left(2t_1^2+3t_1t_2+2t_2^2\right)} \quad (3)$$

$$d = kL^2/2, \quad (4)$$

where L is the cantilever length, t_1 and t_2 are the thickness of the metal coating and silica cantilever, b_1 and b_2 are the

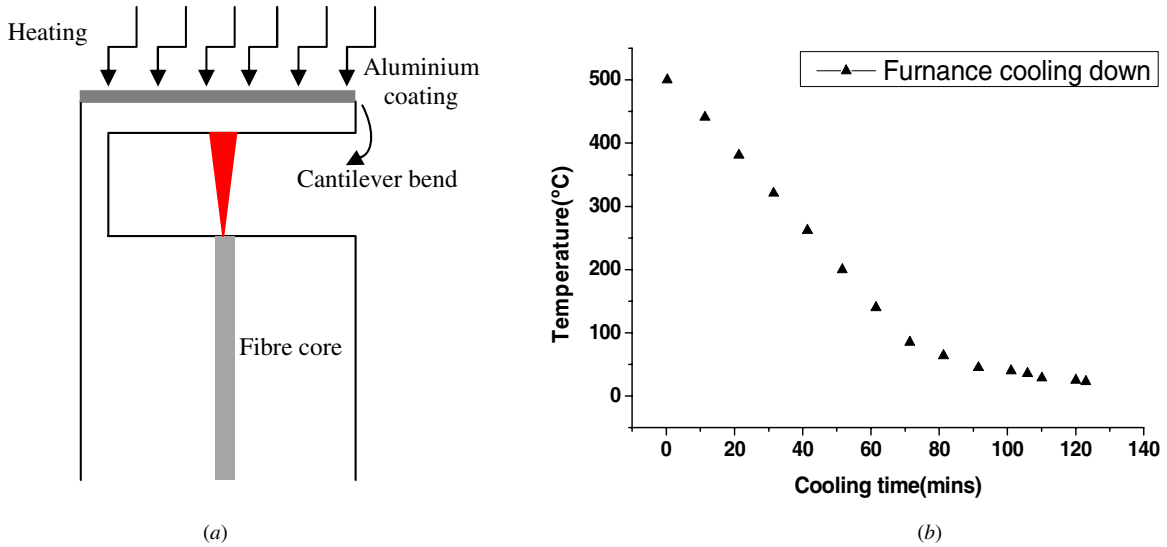

(*a*) (*b*)

Figure 6. (*a*) Experimental set-up of cantilever temperature sensing system. (*b*) Furnace cooling time versus temperature change.

width of coated area and cantilever, k is the cantilever bending curvature, r is the bending radius, α_1 and α_2 are thermal expansion coefficient of coating material and substrate, E_1 and E_2 are Young's modulus of the metal coating and fused silica, and ΔT is the temperature change. Using equation (4), we can predict cantilever tip deflection.

In our experiment, the cantilever is first coated with 4 nm Chrome to aid adhesion and then coated with ~500 nm aluminium. Aluminium is chosen due to its high thermal expansion coefficient compared with fused silica, and ease of deposition. It is assumed that the Aluminium surface tend to oxides to Al_2O_3 in an air environment; however, the deflection caused by this additional layer is very small, and can be ignored. For high temperature sensing application metals with higher melting temperatures will be required.

After functionalizing the top surface of cantilever, we placed the machined optical fibre cantilever into a ceramic tube furnace (LENTON-1200) for temperature cycling. The furnace is then sealed using insulating material in both ends of the heated tube in order to help maintain a stable thermal environment. Here, a thermocouple is employed to monitor the temperature next to the cantilever.

4.2. Temperature sensing

The furnace is heated up to 500 °C and then held at this temperature for half an hour to allow a uniform temperature distribution to form in the ceramic tube. For each temperature cycle the furnace is switched off and allowed to cool down naturally, see figure 6(*b*) for a typical cooling profile. The cantilever deflection during the cooling period is recorded by the interrogation system mentioned in section 3.1, with typical results for two test sensors shown in figure 7. Here, we assume that the aluminium coating layer covered the whole fused silica cantilever, the structure is uniformly heated and no other additional forces are applied to the cantilever. The zero deflection position of cantilever is when cantilever is at room temperature. In our case, all the experiments start at

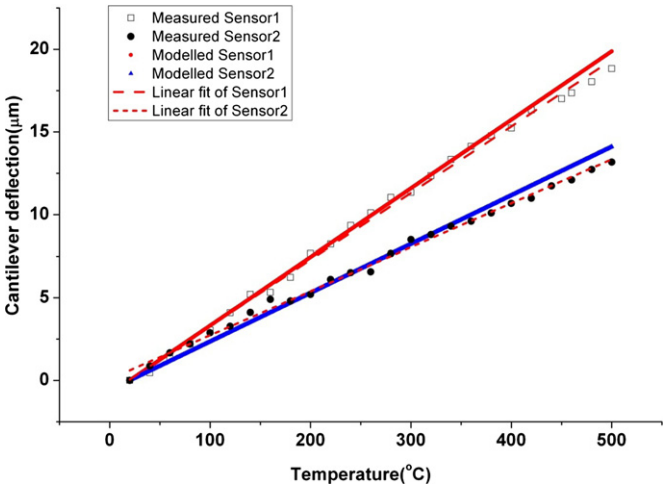

Figure 7. Temperature change versus cantilever deflection change for two temperature sensors.

a room temperature of 20 °C. The cantilever deflection as a function of temperature for two sensors is plotted in figure 7. The solid line represents the model calculated deflection based upon [26] using equations (3) and (4), whereas the individual data-points indicate the measured data. When temperature increases, a surface stress is applied to the cantilever due to the thermal expansion difference between aluminium and fused silica. We believe that the mismatch between the model and linear fit of measured data is probably due to several reasons. The fabricated cantilever is not a perfect rectangular beam with uniform cross-section, which changes the mechanical characteristics. Laser micromachining induced thermal shock [27] might produce the micro-cracks inside the cantilever which will slightly change Young's modulus of the material, and thermal evaporation of aluminium may result in properties that differ from bulk aluminium. According to figure 7, the sensitivity to temperature is given by the gradient of the linear best fit line (dashed line) for each sensor tested, giving sensitivities of 40.2 nm $°C^{-1}$ and 26.5 nm $°C^{-1}$ for sensor 1 and

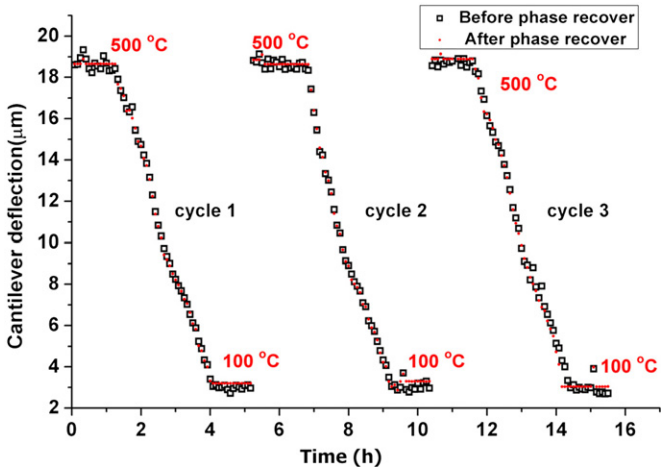

Figure 8. Cantilever deflection versus cooling time.

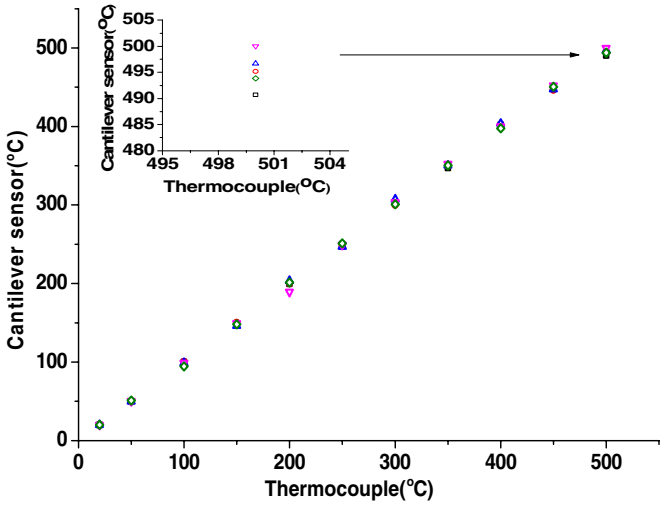

Figure 9. Monitored temperature versus cantilever thermal sensor.

sensor 2, respectively. By using the phase recovered algorithm results in section 3.3, this equals a potential temperature resolution of 0.08 °C and 0.1 °C based upon nm cavity length recovery. The thermal-optic coefficient of air is $\sim 10^{-6}$ K^{-1}; hence, the maximum effective cavity change due to the change of refractive index of air is tens of nanometres over the 500 °C temperature range, which can be ignored here. The difference in temperature sensitivity between the two sensors is due to slightly different cantilever dimensions.

To further investigate the thermal response of the optical fibre cantilever sensor, extended monitoring is carried out with over 16 h, using sensor 1. The temperature was cycled several times from 500 °C to 100 °C, dwelling for at least 1 h at these temperatures. Figure 8 shows the cantilever deflection variations during the whole cycling process. For each cycle a maximum deflection of ~18 μm is found. When the furnace cooled down to room temperature, the cantilever returned to the zero position. When held at 100 °C and 500 °C, we can see from figure 8, temperature noise and fluctuation is reduced nearly ten times due to the phase recovery algorithm. As seen from the figure, the sensor is capable of reliably measuring temperature up to 500 °C.

By using the linear fit from figure 7, we can express the relationship between cantilever deflection and temperature change with the following function:

$$T = 24.8756L + 18.53, \quad (5)$$

where T is the measured temperature in °C and L is the cantilever deflection in micron. Using this calibration, we plot the measured temperature data from 20 °C to 500 °C in figure 9. Here, we can see that the maximum temperature error of ±4.8 °C is found at 500 °C and the rms temperature error calculated by experimental data is ~±1.4 °C over a 500 °C range. These errors are larger than predicted earlier based upon the best case deflection measurement resolution, but reflect the practical experimental conditions which may include time varying temperature drift in the furnace and errors in the thermocouple readout.

5. Conclusion

In conclusion, we demonstrated micro-cantilevers which were fabricated onto the end of a single mode optical fibre by the combination of ps-laser machining and FIB milling techniques. This demonstrated a potential route for rapid manufacture of such cantilevers with the laser fabrication stage taking only a few seconds and the FIB polishing which gives us an optical surface finish. In addition, a phase recovery algorithm is employed to calculate the cantilever deflection with a resolution around 2–3 nm. Finally, we have demonstrated the ability to use this cantilever sensor as a temperature sensor with a near linear fitted deflection response of 40.2 nm $°C^{-1}$, which equates to a temperature resolution of 0.08 °C based upon the best case deflection measurement resolution and a sensing range of up to 500 °C. Extended temperature stability and repeatability was also tested to monitor sensors as they were cycled between 100 °C and 500 °C several times. In this particular test, the maximum experimental temperature error is ~±4.8 °C found at 500 °C, while the average temperature rms error within the whole measurement range is ~±1.4 °C.

The range and performance are set by the particular cantilever dimensions, coating material properties and coating thickness. By optimizing the sensor thickness and functional coating layer, the sensitivity and range can be adjusted. In addition, the micro-cantilever sensor could potentially be integrated with other M(O)EMS devices for temperature measurement in space constraint environment.

Acknowledgments

The authors would like to thank the EPSRC funded IMRC (grant no. EP/F02553X/1) and Renishaw plc. for partial funding of this project and Scottish Universities Physics Alliance provision of a studentship for JL.

References

[1] He S H, Mench M M and Tadigadapa S 2006 Thin film temperature sensor for real-time measurement of electrolyte temperature in a polymer electrolyte fuel cell *Sensors Actuators* A **125** 170–7

[2] Choi H Y, Park K S, Park S J, Paek U C, Lee B H and Choi E S 2008 Miniature fiber-optic high temperature sensor based on a hybrid structured Fabry–Perot interferometer *Opt. Lett.* **33** 2455–7
[3] Kim D H and Kang J 2004 Sagnac loop interferometer based on polarization maintaining photonic crystal fiber with reduced temperature sensitivity *Opt. Express* **12** 4490–5
[4] Ran Z L, Rao Y J, Liu W J, Liao X and Chiang K S 2008 Laser-micromachined Fabry–Perot optical fiber tip sensor for high-resolution temperature- independent measurement of refractive index *Opt. Express* **16** 2252–63
[5] Zhu Y Z, Huang Z Y, Shen F and Wang A B 2005 Sapphire-fiber-based white-light interferometric sensor for high-temperature measurements *Opt. Lett.* **30** 711–3
[6] Canning J, Sommer K and Englund M 2001 Fibre gratings for high temperature sensor applications *Meas. Sci. Technol.* **12** 824
[7] Bandyopadhyay S, Canning J, Stevenson M and Cook K 2008 Ultrahigh-temperature regenerated gratings in boron-codoped germanosilicate optical fiber using 193 nm *Opt. Lett.* **33** 1917
[8] Iannuzzi D, Deladi S, Gadgil V J, Sanders R G P, Schreuders H and Elwenspoek M C 2006 Monolithic fiber-top sensor for critical environments and standard applications *Appl. Phys. Lett.* **88** 053501
[9] Wang H C, Lee C Y and Chiang C M 2007 A MEMS-based air flow sensor with a free-standing micro-cantilever structure *Sensors* **7** 2389–401
[10] Bashir R 2008 BioMEMS: State-of-the-art in detection, opportunities and prospects *Adv. Drug Deliv. Rev.* **56** 1565–86
[11] Dareing D W, Thundat T, Sangmin J and Nicholson M 2005 Modal analysis of microcantilever sensors with environmental damping *J. Appl. Phys.* **97** 084902
[12] Said A A, Dugan M, DeMan S and Iannuzzi D 2008 Carving fiber-top cantilevers with femtosecond laser micromachining *J. Micromech. Microeng.* **18** 035005
[13] Gavan K B, Rector J H, Heeck K, Chavan D, Gruca G, Oosterkamp T H and Iannuzzi D 2011 Top-down approach to fiber-top cantilevers *Opt. Lett.* **36** 2898–900
[14] Timoshenko S 1925 Analysis of bi-metal thermostats *J. Opt. Soc. Am.* **11** 233
[15] Meyer G and Amer N M 1988 Novel optical approach to atomic force microscopy *Appl. Phys. Lett.* **53** 1045–7
[16] Yang Z X, Li X X, Wang Y L, Bao H F and Liu M 2004 Micro cantilever probe array integrated with Piezoresistive sensor *Microelectron. J.* **35** 479–83
[17] Spietz L, Lehnert K W, Siddiqi I and Schoelkopf R J 2003 Primary electronic thermometry using the shot noise of a tunnel junction *Science* **300** 1929–32
[18] Wu L, Cheng T and Zhang Q C 2012 A bi-material microcantilever temperature sensor based on optical readout *Measurement* **45** 1801–6
[19] Gruca G, Man S D, Slaman M, Rector J H and Iannuzzi D 2010 Ferrule-top micromachined devices: design, fabrication, performance *Meas. Sci. Technol.* **21** 094033
[20] Li J, Albri F, Maier R R J, MacPherson W N and Hand D P 2012 Micro-machined optical fibre cantilever as sensor elements *Proc. SPIE* **8428** 842816
[21] Albri F, Li J, Maier R R J, MacPherson W N and Hand D P 2013 Laser machining of sensing components on the end of optical fibres *J. Micromech. Microeng.* **23** 045021
[22] Reyntjens S and Puers R 2001 A review of focused ion beam applications in microsystem technology *J. Micromech. Microeng.* **11** 287
[23] Chen J Y, Chen D J, Geng J X, Li J and Cai H W 2008 Stabilization of optical Fabry–Perot sensor by active feedback control of diode laser *Sensors Actuators* A **148** 376–80
[24] Rao Y J and Jackon D A 1996 Recent progress in fiber optic low-coherence interferometry *Meas. Sci. Technol.* **17** 981–99
[25] Jiang Y 2008 Fourier transform white-light interferometry for the measurement of fiber-optic extrinsic Fabry–Pérot interferometric sensors *IEEE Photon. Technol. Lett.* **20** 75–77
[26] Chu W H, Mehregany M and Mullen R L 1993 Analysis of tip deflection and force of a bimetallic cantilever microactuator *J. Micromech. Microeng.* **3** 4
[27] Hand D P and Russell P S J 1988 Solitary thermal shock waves and optical damage in optical fibers: the fiber fuse *Opt. Lett.* **13** 767–9